

# Atomistic simulations of Mg–Cu metallic glasses: mechanical properties

Nicholas P. Bailey<sup>a,b,\*</sup>, Jakob Schiøtz<sup>a</sup>, Karsten W. Jacobsen<sup>a</sup>

<sup>a</sup> *CAMP, Department of Physics, Technical University of Denmark, DK-2800, Lyngby, Denmark*

<sup>b</sup> *Materials Research Department, Risø National Laboratory, DK-4000, Roskilde, Denmark*

Received 25 August 2003; received in revised form 19 November 2003

## Abstract

The atomistic mechanisms of plastic deformation in amorphous metals are far from being understood. We have derived potential parameters for molecular dynamics simulations of Mg–Cu amorphous alloys using the Effective Medium Theory. We have simulated the formation of alloys by cooling from the melt, and have used these glassy configurations to carry out simulations of plastic deformation. These involved different compositions, temperatures (including zero), and types of deformation (uniaxial strain/pure shear), and yielded stress–strain curves and values of flow stress. Separate simulations were carried out to study specific features in the stress–strain curves associated with transitions involving internal rearrangements of atoms. Energy barriers were calculated as a function of stress, as was the plastic strain associated with events. The latter leads to a characteristic volume of an event which seems to correspond with the derivative of the barrier with respect to stress.

© 2004 Elsevier B.V. All rights reserved.

**Keywords:** Metallic glass; Mg–Cu; Plastic deformation; Atomistic simulation; Localized events; Energy barriers

## 1. Introduction

This paper describes recent and ongoing efforts to study the atomistic processes of plastic deformation in metallic glasses using modern interatomic potentials. The material studied is Cu–Mg, which forms a metallic glass in the composition range 9–42 at.% Cu (complete glass formation over 12–22%, optimal 14.5%). Our interest in this material is due to the closely related ternary alloy Mg<sub>60</sub>Cu<sub>30</sub>Y<sub>10</sub>, which is distinguished by the fact that it is a *bulk* amorphous alloy, or bulk metallic glass (BMG), meaning the cooling rate required to form it is slow enough that relatively large samples can be made. Discovered in the early 1990s by Inoue [1] and Johnson [2] and coworkers, BMGs have been intensely studied since, particularly with regard to finding new BMG-forming systems. Because of the availability of large samples, their mechanical properties are now very relevant and important. However, there is still only limited understanding of their deformation processes.

The phenomena observed in, for example, a uniaxial tensile test of a cylindrical sample at room temperature are

[3,4]: (i) high yield and flow stresses (1.5–2.5 GPa), (ii) no work-hardening; rather strain-softening is observed, which leads to (iii) localization of the strain into intense shear bands which traverse the sample causing finally (iv) complete failure of the sample. It is clear from this phenomenology that shear deformation is the primary mode of interest. Items (i) and (ii) stem directly from the fact that there is no topological defect playing the role of a dislocation in an amorphous metal. The question arises as to what are the elemental events that comprise plastic deformation. Early theories [5] considered them to involve a single atom moving into nearby available space (free volume), with some assistance from the stress field. More recently simulations in two-dimensional systems [6] have shown the events to involve several atoms transforming in a shear-like manner and have led to the formulation of a continuum theory known as the shear transformation zone (STZ) theory, which in its mean-field form has been reasonably successful [6–13].

Our goals in this work are to (i) investigate the phenomenology (e.g. stress–strain curves) of plastic deformation in the simulated glassy systems within computational limits and (ii) determine the basic parameters of an STZ-type theory in the atomistic regime, in the context of a real

\* Corresponding author. Tel.: +45-45-25-32-26; fax: +45-45-93-23-99.  
E-mail address: nbailey@fysik.dtu.dk (N.P. Bailey).

material.<sup>1</sup> That is, we wish to identify and characterize the STZ-like events, in terms of the amount of plastic strain associated with an event, and the energetics of the process (energy barrier, stress-dependence).

## 2. Generating glassy configurations and local atomic structure

The derivation of the EMT potential parameters and the cooling simulations have been described in detail elsewhere [14]. The parameters have been optimized to reproduce cohesive energies, lattice constants and elastic constants of the pure metals, as well as formation energies and some lattice and elastic constants of the intermetallic compounds  $\text{Mg}_2\text{Cu}$  and  $\text{MgCu}_2$ . Glassy samples were produced by cooling from a temperature well above the melting point at  $2.5 \times 10^{11}$  K/s, a rate slow enough to give final configurations quite close to the “ground state” in terms of glassy configurations, and thus, quite stable [14]. The simulations in this work mostly use a composition of 15 at.% Cu, which is close to the optimal glass forming composition, although some data are for a larger range of compositions. In the cooling simulations we observe the glass transition around 350 K for this composition, close to the experimental value [15] of 380 K. Measurements of thermodynamic properties and structure are described in detail in Ref. [14].

## 3. Plastic deformation

We have carried out a range of simulations to determine the plastic response of the glass sample. The first of these were zero-temperature stress–strain measurements under pure shear, done for all glassy compositions. The technique for zero-temperature simulations was as follows: First the configuration resulting from the cooling run was minimized in energy with respect to atomic positions and the size and shape of the periodic box. Then the box-vectors were subjected to increments of strain (in this case pure shear,  $\epsilon_{23}$ ) of 0.0005. Each time the strain was incremented a minimization procedure was carried out to relax all degrees of freedom—atomic positions and strain components—other than the strain component being incremented. The minimization procedure was the MDmin [16] dynamical minimization algorithm. The convergence criterion was that the root-mean-square force on the atoms was less than  $10^{-6}$  eV/Å. For the zero-temperature simulations, the strain history was:  $0 \rightarrow 0.1 \rightarrow -0.1 \rightarrow 0$ . Some stress strain curves are shown in Fig. 1. All curves start at zero stress and strain, with the stress increasing linearly with strain until about 3% shear strain. The slope (twice the shear modulus) increases

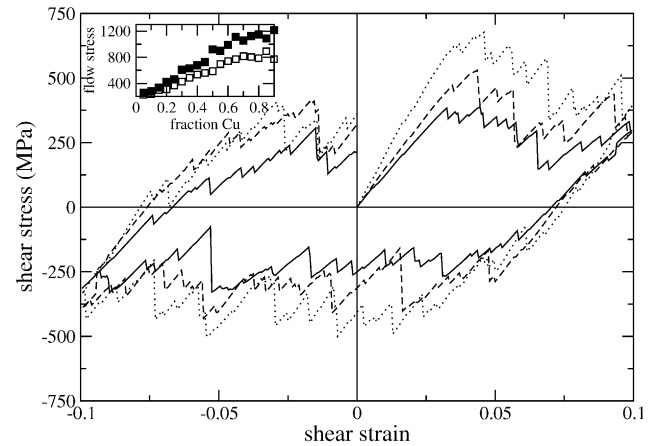


Fig. 1. Stress–strain curves at zero temperature for three compositions: 5, 15 and 25 at.% Cu, solid, dashed and dotted lines, respectively. Inset: composition dependence of zero-temperature flow stress. Filled symbols, increasing strain; open symbols, decreasing strain.

with the amount of Cu, thus the peak stress does also. After the elastic limit of 3%, the stress–strain curve consists of a sequence of linearly increasing sections separated by sharp drops in stress, indicating the occurrence of internal rearrangements which relieve the stress. Investigations of the nature of these rearrangements will be discussed below. Another interesting and possibly important feature is that the peak stresses on the reverse part of the cycle (decreasing strain) are significantly smaller in magnitude than on the increasing side. This indicates some kind of strain softening, which may be part of the mechanism which leads to strain localization in macroscopic samples in experiments. By taking averages of stress over the non-elastic parts of the stress–strain curves, we can determine a flow stress. For increasing strain the average is taken between strains 0.05 and 0.1. For decreasing strain it is taken between 0.05 and  $-0.1$ . These flow stresses are plotted in the inset of Fig. 1, which show more clearly the difference between the increasing and decreasing flow stresses.

The simulations described above differ significantly from experimental measurements in two ways: the very small system-size, and the temperature being zero; at finite temperature the strain-rate also becomes relevant. The jumps in stress seen here do not appear in experimental measurements, presumably because thermal fluctuations allow transitions to occur before the stress reaches such high peaks and because of spatial averaging in the material: the likelihood of the overall stress reaching a high value before some kind of yielding occurs somewhere in the material diminishes as the size of the system increases. We next present data from simulations at finite temperature, at the same system size (2048 atoms). For these simulations a constant temperature and stress MD algorithm was used to simulate the dynamics, subject to the constraint that the component of strain appropriate for the deformation ( $\epsilon_{11}$  for uniaxial strain and  $\epsilon_{23}$  for pure shear) was increased at a fixed rate, specifically

<sup>1</sup> As opposed to two-dimensional materials with model potentials used in the original simulations of Ref. [6].

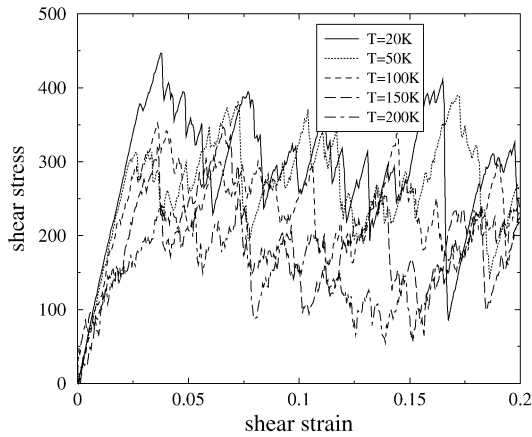


Fig. 2. Stress–strain curves for 15 at.% Cu samples deformed under pure shear at various temperatures, strain rate  $5 \times 10^7 \text{ s}^{-1}$ .

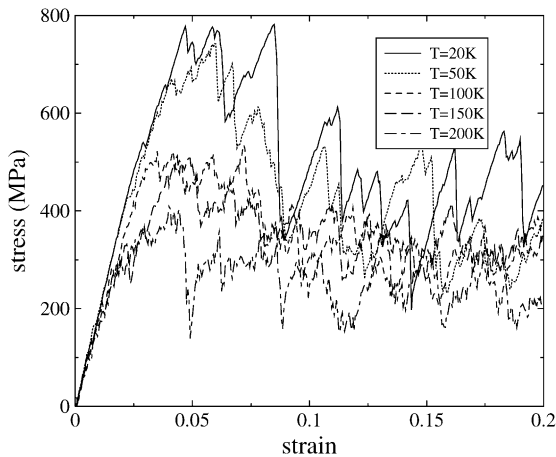


Fig. 3. Stress–strain curves for 15 at.% Cu samples deformed under uniaxial tension at various temperatures, strain rate  $5 \times 10^7 \text{ s}^{-1}$ .

$5 \times 10^7 \text{ s}^{-1}$ . The range of strains was 0 to 0.2, and the stress was averaged over strain intervals of 0.0005. Figs. 2 and 3 show stress–strain curves for compositions 15 at.% Cu, for pure shear and uniaxial strain for temperatures ranging be-

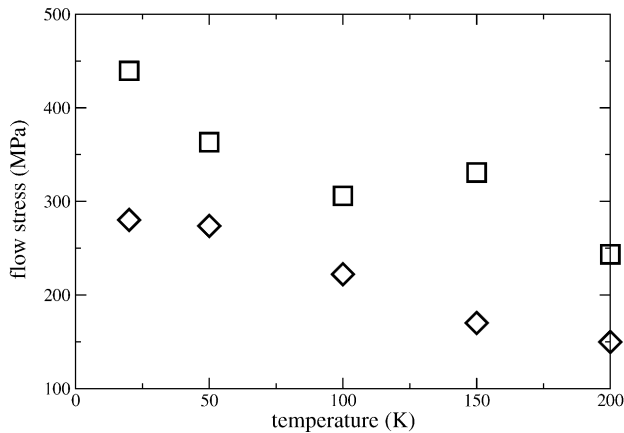


Fig. 4. Finite temperature flow stress for 15% Cu sample. Squares, uniaxial strain; diamonds, pure shear strain.

tween 20 and 200 K. We see that the large jumps persist even at 200 K, thus finite temperature alone is not enough to produce realistic stress–strain curves. By an averaging procedure similar to the one used for the  $T = 0$  data, we can determine the flow stress as a function of temperature. Here the averaging is from strains 0.1 to 0.2, because the initial “yield” stress appears to be significantly higher than the subsequent “flow” stress, which is our current interest. The flow stresses for the 15 at.% Cu sample are shown in Fig. 4.

#### 4. Energy barriers and effective Burgers vectors

In order to study the individual events more closely we have calculated the enthalpy barriers associated with the events taking place during a particular zero-temperature stress–strain simulation. The appropriate means of doing so is in within a constant stress formalism, where all six strain components are true degrees of freedom of the system, and a stress term is added to the energy (making the enthalpy), and to the generalized forces acting on the strain components. The procedure is as follows: starting with configurations saved before and after a plastic event as determined from the stress–strain curve, for each of a range of stresses (including the maximum stress reached before the event occurred and the final stress at the completion of the event), the configurations are minimized with respect to atomic positions and strain-components, under the given constant stress. This gives two local minima of enthalpy separated in the  $3N + \text{six-dimensional}$  configuration space by an enthalpy barrier. We use the nudged elastic band (NEB) method [17–19] to compute the height of this barrier. The result is the barrier height as a function of stress for each event studied. In the NEB calculation, the strain-components, and hence the periodic supercells, differ along the chain; it would be ambiguous to compute real-space difference vectors, so instead we use scaled coordinates for the atomic positions.

For each event and each stress we obtain an enthalpy profile as in Fig. 5; the most important quantity is the barrier itself—the maximum enthalpy of a replica with respect to the initial replica. A second quantity of interest is the difference in strains between the before and after states; this is the amount of plastic strain associated with the event. We can imagine a shear event in an idealized sense by taking a small flat area  $A$  with normal  $\hat{n}$  within the material, cutting the material over this surface, and letting the material on one side of the cut slip with respect to that on the other side of the cut by an amount  $\vec{b}$  (compare to the continuum picture of the nucleation of a dislocation loop with Burgers vector  $\vec{b}$ ). The shear strain felt by the boundary of the system is  $\epsilon_{ij} = (1/2)A(n_i b_j + n_j b_i)/V$ , where  $V$  is the system volume. Since the actual events are not of this form, we cannot identify  $\vec{b}$  and  $A\hat{n}$  directly, but we can infer the symmetrized product  $(1/2)A(n_i b_j + n_j b_i)$  by multiplying the observed plastic strain by  $V$ . This quantity is a symmet-

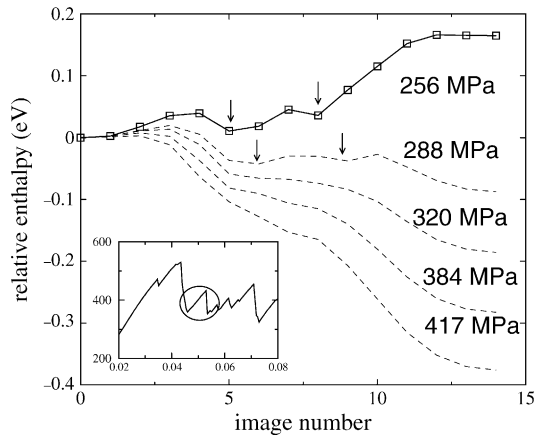


Fig. 5. Enthalpy profiles for various stresses for a particular event during  $T = 0$  shear deformation of a 15% Cu sample. The profiles have been shifted in energy to meet at the initial point. Squares in top profile indicate Nudged Elastic Band replicas of the system. Arrows indicate intermediate minima along the path. Inset shows the part of the stress–strain curve corresponding to this event.

ric tensor with units of volume; the volume is of the order of an atomic volume or bigger; focusing on the 23 component, we call it  $V_{\text{slip}}$ . Another volume that emerges from the barrier computations is the derivative of the energy barrier with respect to stress. Since this is negative, we define the quantity  $V^* = -dE_B/d\sigma$ . In the case of dislocation motion, in particular the motion of a kink, this derivative is of the order of  $b^3$ , which is also the size that  $V_{\text{slip}}$  would be. It is thus of interest whether the volumes are equal for plastic events in an amorphous material.

However, while the plastic strain (inset of Fig. 6) is reasonably independent of stress,  $\epsilon_{\text{pl},23} \sim 0.01 \Rightarrow V_{\text{slip}} \sim 430 \text{ \AA}^3$  (the volume is  $43,000 \text{ \AA}^3$ ), the stress dependence of the barrier is not so clearcut. There is a distinct change of slope visible in Fig. 6 and it is not clear which slope should be compared to  $V_{\text{slip}}$ . The reason for the change of slope is

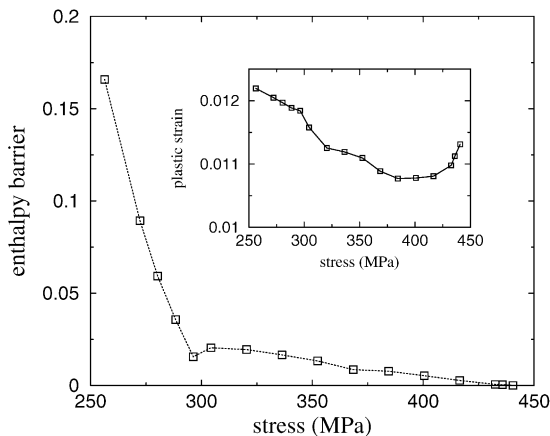


Fig. 6. The enthalpy barrier as a function of stress, for the same event as in Fig. 5. Inset is the 12-component of plastic strain caused by this event, as a function of stress.

clear when one looks at Fig. 5. From the shape of the profile we can see that in fact there are two intermediate minima along the path (arrows in Fig. 5). The “event” in this case can be viewed as three sub-events. The reason they appeared as one is also clear: by the time the barrier for the first event is zero, the barriers for the other two have already vanished and the system simply slides downhill in enthalpy to the final state (all three sub-events having happened). At lower stresses the minima are still there, and at finite temperature one would expect three distinct events. We can also now understand the change of slope of the barrier vs. stress: initially the biggest barrier to the final state is the third one, which has a large stress dependence. Once it becomes lower than the first sub-barrier, the latter becomes dominant, and its stress dependence is much weaker. The associated  $V^*$  parameters are  $\sim 600$  and  $\sim 25 \text{ \AA}^3$ , respectively. Thus it seems reasonable that here  $V_{\text{slip}}$  is perhaps an average of different  $V_{\text{slip}}$  for the three sub-events. To properly determine the connection between  $V^*$  and  $V_{\text{slip}}$  it will be necessary to run separate NEB calculations with the intermediate minima as end-points. This is part of our ongoing work.

## 5. Summary

We have presented the initial stages of a program to study in detail the mechanisms of plastic deformation with atomistic simulations. We have made realistic amorphous configurations by molecular dynamics simulation of cooling from the melt. We have measured stress strain curves at zero temperature and at several non-zero temperatures, and made some progress in analyzing the specific internal rearrangement events that make up the overall deformation.

We have seen that with the small systems and high strain rates that we use, there are large jumps in stress–strain curve. These are not expected to appear in larger systems; we have begun simulations of larger systems (16,384 atoms) and the preliminary data indicate that the large jumps are absent. However, small systems are useful because we can look at the individual events more closely and easily, since the number of degrees of freedom is not too large. In our continuing work we hope to gain more complete understanding of the geometry and energetics of the local plastic deformation events, how they are distributed with regard to quantities such as  $V_{\text{slip}}$  and  $V^*$ , and the way in which they contribute to the overall deformation, particularly as the system size increases.

## Acknowledgements

This work was supported by the Danish Research Councils through Grant No. 5020-00-0012 and by the Danish Center for Scientific Computing through Grant No. HDW-1101-05.

**References**

- [1] A. Inoue, A. Kalo, T. Zhang, S.G. Kim, T. Masumoto, *Mater. Trans. JIM* 32 (1991) 609.
- [2] A. Peker, W.L. Johnson, *Appl. Phys. Lett.* 63 (1993) 2342.
- [3] A.L. Greer, *Science* 267 (1995) 1947.
- [4] W.L. Johnson, *MRS Bull.* 24 (1999) 42.
- [5] F. Spaepen, *Acta Metallurgica* 25 (1977) 407.
- [6] M.L. Falk, J.S. Langer, *Phys. Rev. E* 57 (1998) 7192.
- [7] J.S. Langer, A.E. Lobkovsky, *Phys. Rev. E* 60 (1999) 6978.
- [8] J.S. Langer, *Phys. Rev. E* 62 (2000) 1351.
- [9] J.S. Langer, *Phys. Rev. E* 64 (2001) 011504.
- [10] L.O. Eastgate, J.S. Langer, L. Pechenik, *Phys. Rev. Lett.* 90 (2003) 045506.
- [11] L. Pechenik, J.S. Langer, 2003, cond-mat/0301009.
- [12] L. Pechenik, 2003, cond-mat/0305516.
- [13] J.S. Langer, L. Pechenik, 2003, cond-mat/0301009, v2.
- [14] N.P. Bailey, J. Schiøtz, K.W. Jacobsen, *Simulation of Cu-Mg: Thermodynamics and Structure*, *Phys. Rev. B* 69 (2004) 144205.
- [15] F. Sommer, G. Bucher, B. Predal, *J. Phys. Colloque C8* 41 (1980) 563.
- [16] P. Stoltze, *Simulation Methods in Atomic Scale Materials Physics*, Polyteknisk Forlag, Lyngby, Denmark, 1997.
- [17] G.M.H. Jónsson, K.W. Jacobsen, in: B.J. Berne, G. Ciccotti, D.F. Coker (Eds.), *Classical and Quantum Dynamics in Condensed Phase Simulations*, World Scientific, 1998.
- [18] G. Henkelman, H. Jónsson, *J. Chem. Phys.* 113 (2000) 9978.
- [19] G. Henkelman, B. Uberuaga, H. Jónsson, *J. Chem. Phys.* 113 (2000) 9901.